Absolute configuration of a [1]rotaxane determined from vibrational and electronic circular dichroism spectra

Andrew R Puente, Adrien Bessaguet, Noël Pairault, Grégory Pieters, Jeanne Crassous, Prasad Polavarapu, Isabelle Opalinski, Sébastien Papot

Absolute configuration of a [1]rotaxane determined from vibrational and electronic circular dichroism spectra

Andrew R. Puente,[a] Adrien Bessaguet,[b] Noël Pairault,[b] Grégory Pieters,[c] Jeanne Crassous,*[d] Prasad L. Polavarapu,*[a] Isabelle Opalinski,*[b] Sébastien Papot*[b]

Abstract: The experimental vibrational circular dichroism (VCD) and electronic circular dichroism (ECD) spectra were measured for the enantiomers of [1]rotaxane **1**. These experimental spectra have been analyzed using predicted VCD and ECD spectra for (*S*, R_{mp}) or (*S*, S_{mp}) diastereomers using density functional theory. This comparison allowed for a definitive assignment of the absolute configuration of **1**.

Keywords: Rotaxane, absolute configuration, density functional theory, vibrational circular dichroism, electronic circular dichroism, mechanical planar chirality

Introduction

While many interlocked molecules, such as rotaxanes and catenanes, have been described in the literature over the last 30 years,[1-8] only little attention has been paid to the stereoselective synthesis of mechanically chiral rotaxanes to date[9]. In 2014, Goldup and co-workers reported the first method enabling the access to mechanically planar chiral (MPC)[10] [2]rotaxanes without using chiral separation techniques.[11] Soon after, they accomplished the diastereoselective synthesis of MPC [2]rotaxanes through the active template Cu-mediated alkyne–azide cycloaddition (AT-CuAAC)[12,13] reaction.[14] Recently, Leigh and co-workers developed a single-step enantioselective strategy leading to MPC [2]rotaxane enantiomers in 50% ee.[15] The emergence of novel stereoselective approaches has also highlighted the lack of techniques allowing the assignment of the absolute configuration of such rotaxanes, in most cases determined using single crystal X-ray diffraction. However, obtaining suitable crystals remains highly challenging, pointing out the need to design alternative methods for assigning the absolute mechanical configuration of these interlocked chiral molecules. Within this framework, Goldup and Buma demonstrated that vibrational circular dichroism (VCD) spectroscopy has the potential to determine the absolute stereochemistry of such architectures.[16] Indeed, they showed that computed VCD spectra were in accordance with the corresponding experimental ones, thereby providing a very useful means to resolve the absolute configuration of MPC [2]rotaxanes.

Very recently, we reported on the first diastereoselective synthesis of [1]rotaxane using the AT-CuAAC reaction.[17] This method enabled the preparation of mirror-image MPC [1]rotaxanes with a high stereoselectivity. In this approach, the mechanically planar chirality of the obtained [1]rotaxanes **1** was guided by the absolute configuration of the covalent stereogenic center attached at the base of the macrocycle. However, as we failed to produce a single-crystal, we were unable to attribute the absolute stereochemistry, either (*S*, R_{mp}) or (*S*, S_{mp}),[18] of the major isomer (Figure 1).

In this article, we report the absolute configuration (AC) of **1** determined using vibrational circular dichroism (VCD) and electronic circular dichroism (ECD) spectra. Circular dichroism is the differential absorption of left and right circularly polarized incident light.[19] ECD probes the CD in electronic transitions,[19] while VCD probes that in vibrational transitions.[20-23] We present the experimental VCD and ECD spectra for (*S*)-**1** and (*R*)-**1** and their comparison to corresponding predicted spectra for (*S*, R_{mp}) or (*S*, S_{mp}) diastereomers. The predicted spectra were obtained using density functional theory (DFT). This comparison analysis allowed us to establish the hitherto unknown AC of **1**.

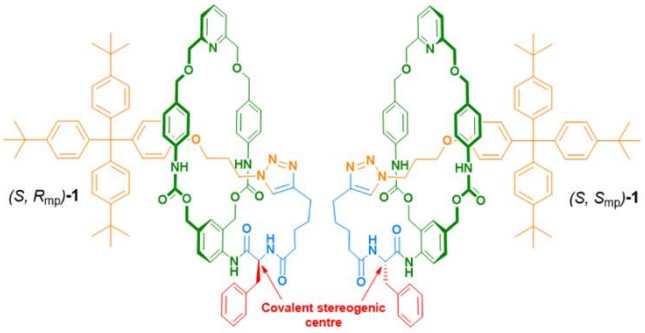

Figure 1 Structures of the two possible diastereomers of [1]rotaxane (*S*)-**1**.

Computational Methods

Initial conformational searches were performed with Conflex program[24] using interlocked starting geometries for the

[a] *Dr. A. R. Puente, Prof. P. L. Polavarapu, Department of Chemistry, Vanderbilt University, Nashville, TN 37235, USA. E-mail: Prasad.L.Polavarapu@vanderbilt.edu*
[b] *Dr. A. Bessaguet, Dr. N. Pairault, Dr. I. Opalinski, Prof. S. Papot, Université de Poitiers, UMR CNRS 7285, Institut de Chimie des Milieux et des Matériaux de Poitiers (IC2MP), Groupe « Système Moléculaires Programmés », 4 rue Michel Brunet, TSA 51106, 86073 Poitiers Cedex 9, France. E-mail: isabelle.opalinski@univ-poitiers.fr, sebastien.papot@univ-poitiers.fr*
[c] *Dr. G. Pieters, Université Paris-Saclay, CEA, INRAE, Département Médicaments et Technologies pour la Santé (DMTS), SCBM, F-91191, Gif-sur-Yvette, France*
[d] *Dr. J. Crassous, Univ. Rennes, Institut des Sciences Chimiques de Rennes, UMR CNRS, 6226 Campus de Beaulieu, F-35042 Rennes cedex, France. E-mail: jeanne.crassous@univ-rennes1.fr*

diastereomers, (*S*, R_{mp})- and (*R*, R_{mp})-**1**, in a 10 kcal.mol^{-1} energy window. This search produced many structures without a mechanical stereogenic unit, so a second search was performed using the lowest energy interlocked conformation from the first search. This second search provided many low-energy conformations for both diastereomers, with interlocked conformations being identified as the lowest energy structures There were 2650 conformers for (*S*, R_{mp})-**1** in in 10 kcal.mol^{-1} window. For (*R*, R_{mp})-**1**, since there were only 321 conformers in 10 kcal.mol^{-1} window, we examined 870 conformers in 20 kcal.mol^{-1} window. Subsequent hand-filtering of the (*R*, R_{mp})-1 structures, for eliminating the non-interlocked structures, resulted in 430 interlocked structures and these structures were used for quantum mechanical (QM) calculations. All of 2650 (*S*, R_{mp})-**1** structures were used for QM calculations, without any hand-filtering. This process was repeated using the (*R*, S_{mp})- and (*S*, S_{mp})-**1** structures, but no additional conformations were found.

The numerous conformations and the large size of the [1]rotaxane diastereomers rendered QM calculations time consuming and computer intensive. Following the work of Koenis et al.,[16] we performed an initial geometry optimization using a density functional tight-binding (DFTB) method with the 3ob-3-1 parameter set[25] to identify lower energy structures prior to moving onto more time-consuming DFT optimization and frequency calculations. The DFTB-optimized structures in the lowest 2 kcal.mol^{-1} energy window were selected for further processing. Again hand-filtering, for eliminating non-interlocked structures, resulted in 456 interlocked conformations for (*S*, R_{mp})- and 92 for (*R*, R_{mp})-**1**, which were carried over for DFT optimization using the B3LYP functional[26,27] and 6-31G* basis set.[28] VCD and ECD calculations were then performed on the 76 (*S*, R_{mp})- and 33 (*R*, R_{mp})-**1** optimized conformations in the lowest 2 kcalmol^{-1} energy window. The lowest energy conformer (#269 in the list of conformers generated by Conflex) of (*S*, R_{mp}) diastereomer is displayed in Figure 2.

All QM calculations were performed using Gaussian 16.[29] Vibrational animations and electron density maps were generated using GaussView program[30]. The VCD and ECD spectra were simulated using CDSpecTech[31,32] and contributing conformers were weighted by their Gibb's energies for all spectra. The VCD and ECD spectra for (*R*, R_{mp})-**1** were each multiplied by -1 to generate those for (*S*, S_{mp})-**1**.

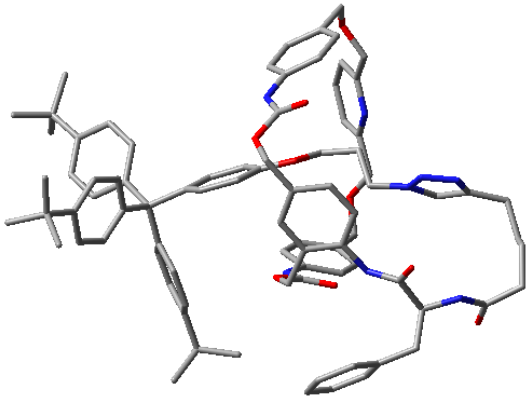

FIGURE 2. Lowest Gibb's Energy conformer of (*S*, R_{mp})-1. Hydrogen atoms are not shown for clarity.

Results and Discussion

VCD SPECTRAL ANALYSIS

Two separate experimental VCD measurements were performed on (*S*)- and (*R*)-**1**, first with 3000 scans and then another with 9000 scans. Since experimental VCD signals were weak, a weighted average of these two measurements was taken, with each measurement weighted by $\sqrt{N}$, where *N* is the number of scans used for the measurement. The resulting VCD spectra (Figure 3a) have a sharp mirror-image band at ~1540 cm^{-1} and small bands at ~1246, 1207, 1200 and 1041 cm^{-1}.

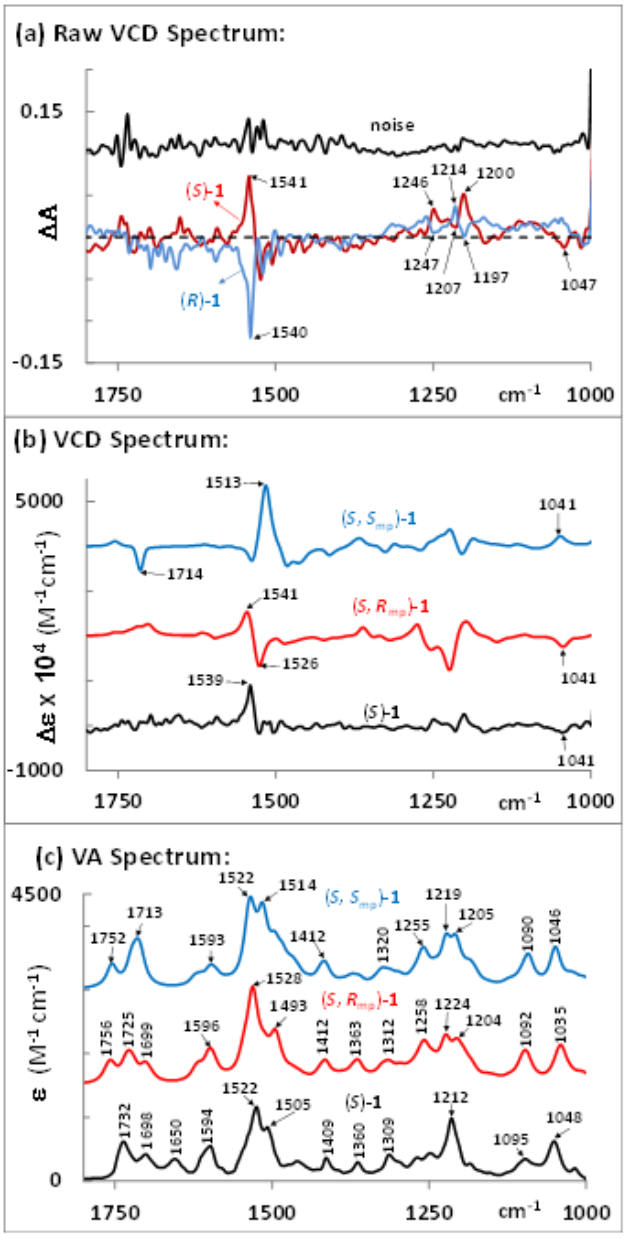

FIGURE 3 (a) Experimental VCD spectra of solvent subtracted (*S*)- and (*R*)-**1** and associated noise level. (b) VCD spectrum of (*S*)-**1**, obtained as one-half the difference between enantiomer spectra, and the predicted spectra of (*S*, R_{mp})- and (*S*, S_{mp})-**1** at the B3LYP/6-31G* level. (c) Experimental vibrational absorption (VA) spectrum of (*S*)-1, and corresponding predicted spectra for (*S*, R_{mp})- and (*S*, S_{mp})-**1**. All simulated frequencies were scaled by 0.97.

The VCD spectrum for (*S*)-**1**, obtained as one-half the difference between enantiomer spectra is compared to those predicted for (*S*, R_{mp}) and (*S*, S_{mp}) diastereomers in Figure 3b. The experimental VCD spectrum of (*S*)-**1** has positive VCD band at 1539 cm^{-1} and there is a hint of adjacent negative VCD at ~1520 cm^{-1}, but it is barely above the noise level. The predicted VCD spectrum for (*S*, R_{mp}) shows positive band at 1541 cm^{-1} and negative band at 1526 cm^{-1}, both of roughly equal magnitudes.

The predicted VCD spectrum for (*S*, S_{mp}) shows a triplet of neighboring bands, with large positive at 1513 cm^{-1} and two weak negative bands one on each side. It is somewhat difficult to draw a definitive conclusion on the AC of **1** based solely on this region of the experimental VCD spectrum.

However, there are two experimental VCD bands that have favorable comparisons with those in the predicted spectrum for (*S*, R_{mp}), but not in that for (*S*, S_{mp}).

(a). No significant VCD is apparent in the experimental spectrum in the amide I region (~1700 cm^{-1}). The asymmetric stretch of both amides near the stereocenter has a scaled frequency of 1702 cm^{-1} for (*S*, R_{mp}). The associated rotational strength is weak, so much so that it is barely visible in the simulated VCD spectrum for (*S*, R_{mp}). This prediction is in line with the experimental observation. In contrast to this experimental observation, the VCD spectrum of (*S*, S_{mp})-**1** has a sharp negative VCD band at 1714 cm^{-1}. Visualization of vibrations of (*S*, S_{mp})-**1** indicates that 1714 cm^{-1} band arises from the amide group that connects the stereocenter to the macrocycle.

(b). The negative experimental VCD band at 1041 cm^{-1} is reproduced in the predicted spectrum for (*S*, R_{mp})-**1**, while the corresponding band for (*S*, S_{mp})-**1** has opposite sign. Visualization of vibrations reveals that 1041 cm^{-1} band is a result of CH rocking along the lasso portion of the rotaxane, specifically between the alkyl chain connecting the stereocenter and the triazole heterocycle.

Based on these two observations, the experimental VCD spectrum of (*S*)-**1** can be preferentially associated with the (*S*, R_{mp}) diastereomer. To ensure that this conclusion will not be altered at higher level calculations, we have undertaken VCD calculations using BP86 functional[33] and TZVP basis set[34] for the lowest energy conformers of (*S*, R_{mp})- and (*S*, S_{mp})-**1**. These spectra, found to be similar to the ones presented in Figure 3, are delegated to Supporting Information. The nature of vibrations associated with scaled frequencies of 1546, 1521 and 1041 cm^{-1} are depicted in Figure 4.

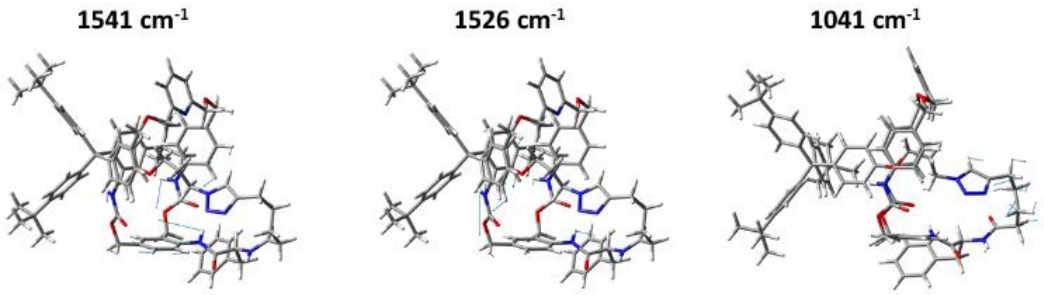

Figure 4. Depiction of atomic displacements associated with scaled frequencies of 1541, 1526 and 1041 cm^{-1} for (*S*, R_{mp}) diastereomer, as obtained from GaussView program.[30]

ECD SPECTRAL ANALYSIS

We have previously reported the experimental ECD spectra of (*S*)- and (*R*)-**1** along with their synthesis.[17] The experimental spectra contain three clear mirror-image bands for enantiomers, in the 220 to 300 nm region, with (*S*)-**1** showing negative-positive-negative sequence of ECD bands. The simulated ECD spectra of (*S*, R_{mp})- and (S, S_{mp})-**1** appear as near mirror-image spectra, despite their diastereomeric relationship. This may indicate that the ECD contribution of the mechanically planar stereogenic unit is much greater than that of the stereocenter, a phenomenon that has been reported for axial chirality.[35] The simulated ECD spectrum of (*S*, R_{mp})-**1** better matches the experimental ECD spectrum, than (*S*, S_{mp})-**1**, with negative-positive-negative sequence of bands observed for (*S*)-**1** being reproduced in the simulated spectrum (Figure 5).

The simulated spectrum of (*S*, R_{mp})-**1** is a result of two distinct classes of conformers, one set with two ECD bands and another set with three (Figure 6). To discuss MO contributions to the simulated ECD spectrum of (*S*, R_{mp}), we focus our analysis on two lowest energy structures of (*S*, R_{mp})-**1**, conformers C269 and C463, which serve as representatives of these two classes and are also the two lowest energy structures of (*S*, R_{mp}), with roughly equal populations (~5% by Gibb's energy).

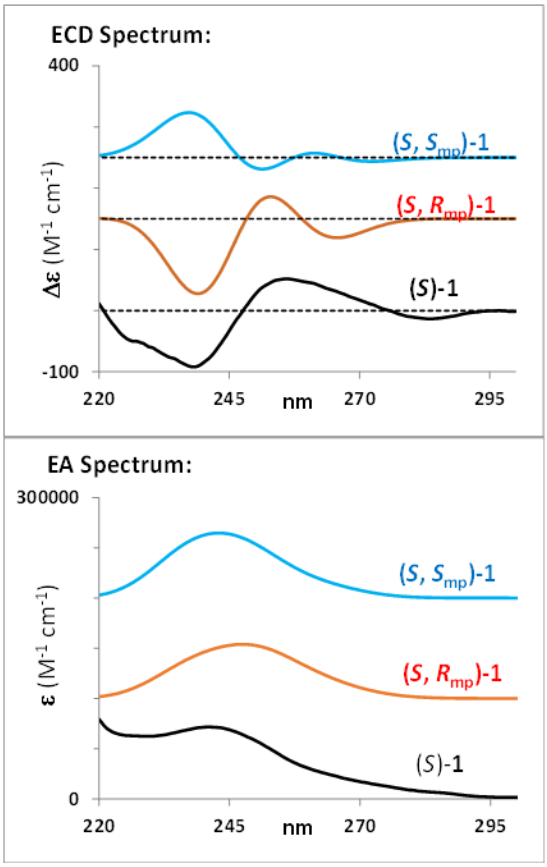

FIGURE 5 Smoothed experimental ECD and EA spectra of (*S*)-**1** (black) and the simulated spectra of (*S*, R_{mp})-**1** (red) and (*S*, S_{mp})-**1** (blue) at the B3LYP/6-31G* level. Conformers are weighted by their Gibb's energies. The intensity of the experimental ECD spectrum has been multiplied by 3 for visibility and the simulated ECD and EA spectra have their wavelengths scaled by 1.01.

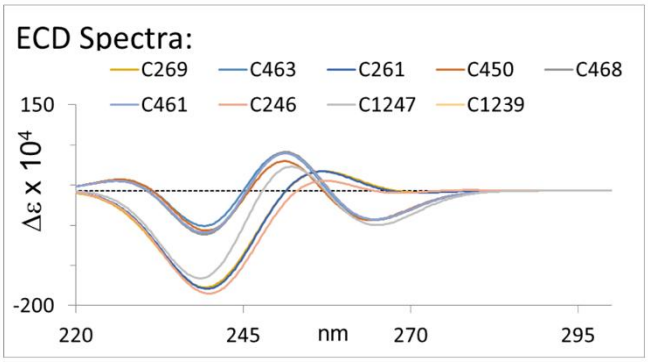

FIGURE 6 Simulated ECD spectra for the lowest energy structures of (*S*, R_{mp})-**1**. These nine structures account for ~38% of the population by Gibb's energy. The horizontal ordering of conformer numbers in the legend matches ordering by Gibb's energy, with C269 and C463 being the lowest energy conformers.

The ECD bands of interest for conformers C269 and C463 are a result of excited states that involve many molecular orbitals (MOs), which obscured the nature of their origin. To further investigate these transitions, we generated the Natural Transition Orbitals (NTOs)[36] of the excited states that contributed the most overall to the ECD spectrum for C269 and C463. This analysis reveals that conformer C269 has an intense π-π* ECD band centered at ~240 nm. This band is a result of a transition from a π MO along the macrocycle to a π* MO on the stopping group, but this also includes some contribution from the lower portion of the macrocycle (Figure 7). There is another π-π* ECD band centered at ~260 nm that is a result of MO contributions from the macrocycle near where the mechanical stereogenic unit originates (Figure 8).

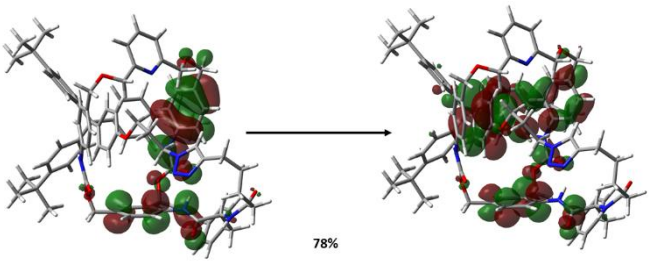

Figure 7. Natural Transition Orbitals for the 240 nm ECD band of conformer C269. The electron density in ground state MO is on the left, and that in the corresponding excited state MO is on the right. The contribution from this pair is ~78%.

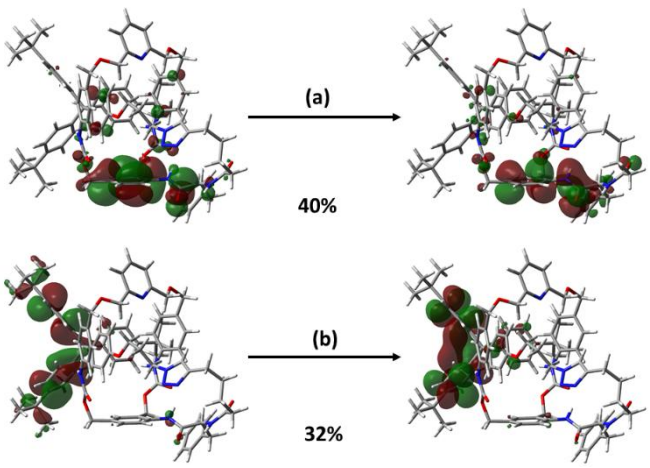

Figure 8. Natural Transition Orbitals for the 260 nm ECD absorption band for conformer C269. The electron density in ground state MO is on the left, and that in the corresponding excited state MO is on the right. The contribution from the top pair (a) is ~40% and that from the bottom pair (b) is 32%.

Conformer C469 has three ECD bands of roughly equal intensity at 240, 250, and 265 nm. There is a π-π* band centered at 240 nm that, much like the 240 nm C269 band, involves a transition from a π MO from the macrocycle to a π* MO on the stopper. NTO analysis reveals an additional contributing π-π* transition localized on the left-hand side of the macrocycle (Figure 9b). The second ECD band is another π-π* centered at 250 nm. NTO analysis decomposes the transition into three pairs of MOs, each with roughly equal occupancy ~30%) (see Figure 10). Electron density pictures for 265 nm ECD band are displayed in Figure 11.

The simulated ECD bands for (*S*, R_{mp})-**1** show great agreement at the B3LYP/6-31G* level, a level of theory that has been shown to have large errors for charge-transfer interactions in the calculation of Rydberg states.[37-39] To test the validity of our results at the B3LYP/6-31G* level, we carried out additional single-point TD-DFT calculations on the lowest energy structures of (*S*, R_{mp})- and (*S*, S_{mp})-**1** at the CAM-B3LYP/6-31G* level using the previously calculated B3LY/6-31G* optimized geometries. CAM-B3LYP has been shown to predict excited-states with better accuracy than B3LYP thanks to the addition of a long-range correction.[40] The corresponding simulated spectra are presented in Figure 12. The computed transition wavelengths require a much larger scale factor (1.075) to be consistent with experiment than the B3LYP transition wavelengths (1.01). However, the calculations reproduce the trend from the B3LYP/6-31G* level, giving near mirror-image signs for ECD bands between (*S*, R_{mp}) and (*S*, S_{mp}). In addition, the negative-positive-negative ECD triplet at 240, 255, and 265 nm for (*S*, R_{mp}) is simulated with matching signs observed in the experimental spectrum of (*S*)-**1**.

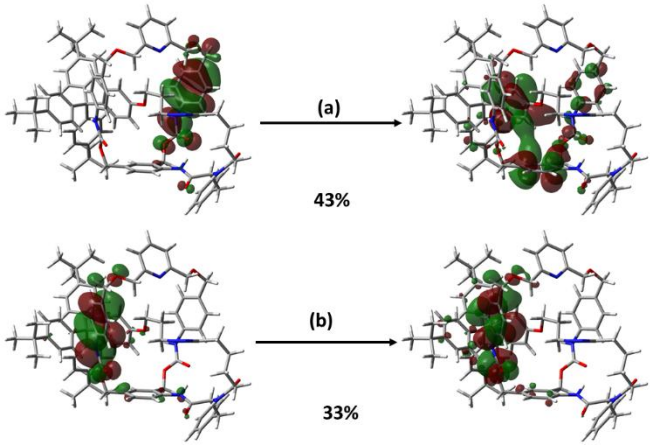

Figure 9. Natural Transition Orbital pairs for the 240 nm band for conformer C463. Ground state MO density is on the left and the corresponding excited state density is on the right. (a). The contribution from the top pair (a) is 43% and that from the bottom pair (b) is 33%.

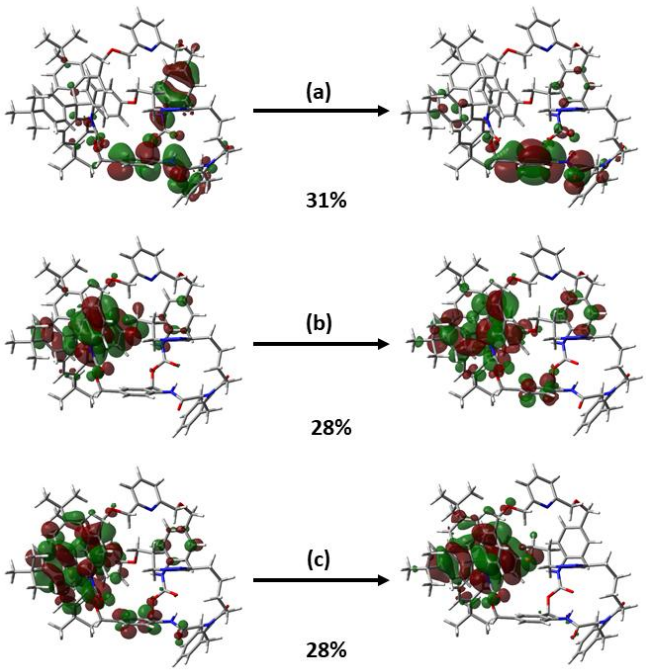

Figure 10. Natural Transition Orbitals for the 250 nm band of C463. On the left are the ground state densities and on the right are the excited-state densities. The contribution from each pair of MOs is roughly the same (~30%).

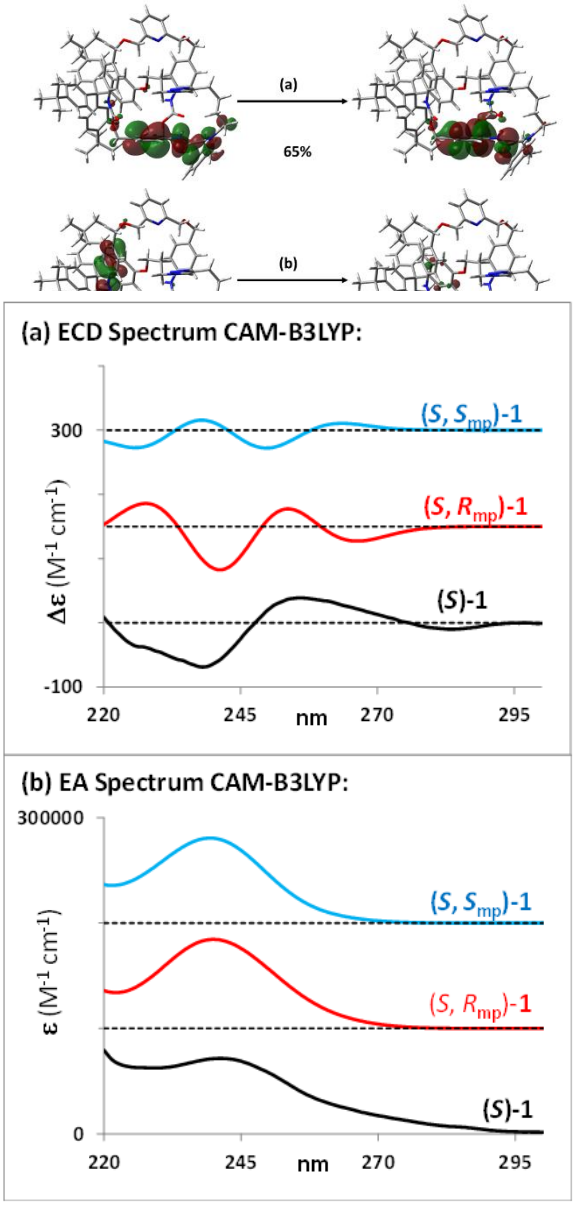

Figure 11. Natural Transition Orbitals for the 265 nm transition of conformer C463. On the left are the ground state densities and on the right are the excited-state densities. Occupancy for the top pair is ~65% and is ~32% for the bottom pair.

Figure 12. Smoothed experimental ECD and EA spectra of (*S*)-**1** (black) and the simulated spectra of (*S*, R_{mp})-**1** (red) and (*S*, S_{mp})-**1** (blue) at the CAM-B3LYP/6-31G* level. Conformers are weighted by their Gibb's energies. The intensity of the experimental ECD spectrum has been multiplied by 3 for visibility and the simulated ECD and EA spectra have their wavelengths scaled by 1.075.

Conclusions

Based on the comparison of experimental VCD spectrum of (*S*)-**1** with those predicted for (*S*, R_{mp}) and (*S*, S_{mp}) diastereomers there is some evidence for associating (*S*)-1 with (*S*, R_{mp}). This AC was confirmed by the comparison of experimental ECD spectrum of (*S*)-**1** with those predicted for (*S*, R_{mp}) and (*S*, S_{mp}) diastereomers. Thus, the current VCD and ECD spectroscopic investigation leads to definitive assignment of AC associated with mechanically planar stereogenic unit in [1]rotaxanes.

Acknowledgments

We thank the Ministère de l'Education Nationale, de la Recherche et de la Technologie and the Centre National de la Recherche Scientifique (CNRS). This work was conducted in part using the resources of the Advanced Computing Center for Research and Education (ACCRE) at Vanderbilt University.

Supporting information

Calculated VCD spectra at BP86/TZVP level.

This information may be found in the online version of this article at the publisher's website.

REFERENCES AND NOTES

1. Bruns CJ, Stoddart JF. The Nature of the Mechanical Bond: From Molecules to Machines. New York: Wiley; 2016.
2. Waelès P, Gauthier M, Coutrot F. Challenges and Opportunities in the Post-Synthetic Modification of Interlocked Molecules. Angewandte Chemie International Edition 2020; https://doi.org/10.1002/anie.202007496.
3. Denis M, Goldup SM. The active template approach to interlocked molecules. Nature Reviews Chemistry 2017;1(8):0061.
4. Fielden SDP, Leigh DA, Woltering SL. Molecular Knots. Angewandte Chemie International Edition 2017;56(37):11166-11194.
5. Lewis JEM, Beer PD, Loeb SJ, Goldup SM. Metal ions in the synthesis of interlocked molecules and materials. Chemical Society Reviews 2017;46(9):2577-2591.
6. Gil-Ramírez G, Leigh DA, Stephens AJ. Catenanes: Fifty Years of Molecular Links. Angewandte Chemie International Edition 2015;54(21):6110-6150.
7. Beves JE, Blight BA, Campbell CJ, Leigh DA, McBurney RT. Strategies and Tactics for the Metal-Directed Synthesis of Rotaxanes, Knots, Catenanes,

and Higher Order Links. Angewandte Chemie International Edition 2011;50(40):9260-9327.
8. Crowley JD, Goldup SM, Lee A-L, Leigh DA, McBurney RT. Active metal template synthesis of rotaxanes, catenanes and molecular shuttles. Chemical Society Reviews 2009;38(6):1530-1541.
9. Maynard JRJ, Goldup SM. Strategies for the Synthesis of Enantiopure Mechanically Chiral Molecules. Chem 2020;6(8):1914-1932.
10. Jamieson EMG, Modicom F, Goldup SM. Chirality in rotaxanes and catenanes. Chemical Society Reviews 2018;47(14):5266-5311.
11. Bordoli RJ, Goldup SM. An Efficient Approach to Mechanically Planar Chiral Rotaxanes. Journal of the American Chemical Society 2014;136(13):4817-4820.
12. Aucagne V, Berná J, Crowley JD, Goldup SM, Hänni KD, Leigh DA, Lusby PJ, Ronaldson VE, Slawin AMZ, Viterisi A and others. Catalytic "Active-Metal" Template Synthesis of [2]Rotaxanes, [3]Rotaxanes, and Molecular Shuttles, and Some Observations on the Mechanism of the Cu(I)-Catalyzed Azide−Alkyne 1,3-Cycloaddition. Journal of the American Chemical Society 2007;129(39):11950-11963.
13. Aucagne V, Hänni KD, Leigh DA, Lusby PJ, Walker DB. Catalytic "Click" Rotaxanes: A Substoichiometric Metal-Template Pathway to Mechanically Interlocked Architectures. Journal of the American Chemical Society 2006;128(7):2186-2187.
14. Jinks MA, de Juan A, Denis M, Fletcher CJ, Galli M, Jamieson EMG, Modicom F, Zhang Z, Goldup SM. Stereoselective Synthesis of Mechanically Planar Chiral Rotaxanes. Angewandte Chemie International Edition 2018;57(45):14806-14810.
15. Tian C, Fielden SDP, Pérez-Saavedra B, Vitorica-Yrezabal IJ, Leigh DA. Single-Step Enantioselective Synthesis of Mechanically Planar Chiral [2]Rotaxanes Using a Chiral Leaving Group Strategy. Journal of the American Chemical Society 2020;142(21):9803-9808.
16. Koenis MAJ, Chibueze CS, Jinks MA, Nicu VP, Visscher L, Goldup SM, Buma WJ. Vibrational circular dichroism spectroscopy for probing the expression of chirality in mechanically planar chiral rotaxanes. Chemical Science 2020;11(32):8469-8475.
17. Pairault N, Bessaguet A, Barat R, Frédéric L, Pieters G, Crassous J, Opalinski I, Papot S. Diastereoselective synthesis of [1]rotaxanes via an active metal template strategy. Chemical Science 2021;12(7):2521-2526.
18. When the absolute configuration of the stereogenic covalent center was *S*, the configurations of the two potential diastereoisomers were either (*S*, *R*mp) or (*S*, *S*mp). See Figure 1.
19. Berova N, Polavarapu PL, Nakamishi K, Woody RW. Comprehensive Chiroptical Spectroscopy. New York: Wiley; 2012.
20. Polavarapu PL. Chiroptical Spectroscopy: Fundamentals and Applications: CRC Press LLC; 2016.
21. Nafie LA. Vibrational Optical Activity: Principles and Applications. New York: John Wiley and Sons; 2011.
22. Stephens PJ, Devlin F, Cheeseman JR. VCD Spectroscopy for Organic Chemists: CRC Press; 2012.
23. Barron LD. Molecular light scattering and optical activity. Cambridge: Cambridge University Press; 2004.
24. Conflex. High performace conformation analysis. Tokyo; 2000.
25. Gaus M, Goez A, Elstner M. Parametrization and Benchmark of DFTB3 for Organic Molecules. Journal of Chemical Theory and Computation 2013;9(1):338-354.
26. Lee C, Yang W, Parr RG. Development of the Colle-Salvetti correlation-energy formula into a functional of the electron density. Physical Review B 1988;37(2):785-789.
27. Becke AD. Density-functional thermochemistry. III. The role of exact exchange. The Journal of Chemical Physics 1993;98(7):5648-5652.
28. Hehre WJ, Ditchfield R, Pople JA. Self—Consistent Molecular Orbital Methods. XII. Further Extensions of Gaussian—Type Basis Sets for Use in Molecular Orbital Studies of Organic Molecules. The Journal of Chemical Physics 1972;56(5):2257-2261.
29. Frisch MJ, Trucks GW, Schlegel HB, Scuseria GE, Robb MA, Cheeseman JR, Scalmani G, Barone V, Petersson GA, Nakatsuji H and others. Gaussian 16 Rev. C.01. Wallingford, CT; 2016.
30. Dennington R, Keith TA, Millam JM. GaussView, Version 6.1 Shawnee Mission, KS: Semichem Inc.; 2016.
31. Covington CL, Polavarapu PL. CDSpecTech: Computer Programs for Calculating Similarity Measures for Experimental and Calculated Dissymmetry Factors and Circular Intensity Differentials https://sites.google.com/site/cdspectech1/; 2016.
32. Covington CL, Polavarapu PL. CDSpecTech: A single software suite for multiple chiroptical spectroscopic analyses. Chirality 2017;29(5):178-192.
33. Becke AD. Density-functional exchange-energy approximation with correct asymptotic behavior. Physical Review A 1988;38(6):3098-3100.
34. Schäfer A, Huber C, Ahlrichs R. Fully optimized contracted Gaussian basis sets of triple zeta valence quality for atoms Li to Kr. The Journal of Chemical Physics 1994;100(8):5829-5835.
35. Polavarapu PL, Jeirath N, Kurtán T, Pescitelli G, Krohn K. Determination of the absolute configurations at stereogenic centers in the presence of axial chirality. Chirality 2009;21(1E):E202-E207.
36. Martin RL. Natural transition orbitals. The Journal of Chemical Physics 2003;118(11):4775-4777.
37. Peach MJG, Benfield P, Helgaker T, Tozer DJ. Excitation energies in density functional theory: An evaluation and a diagnostic test. The Journal of Chemical Physics 2008;128(4):044118.
38. Raeber AE, Wong BM. The Importance of Short- and Long-Range Exchange on Various Excited State Properties of DNA Monomers, Stacked Complexes, and Watson–Crick Pairs. Journal of Chemical Theory and Computation 2015;11(5):2199-2209.
39. Mahato B, Panda AN. Assessing the Performance of DFT Functionals for Excited-State Properties of Pyridine-Thiophene Oligomers. The Journal of Physical Chemistry A 2021;125(1):115-125.
40. Yanai T, Tew DP, Handy NC. A new hybrid exchange–correlation functional using the Coulomb-attenuating method (CAM-B3LYP). Chemical Physics Letters 2004;393(1):51-57.

Graphical Abstract

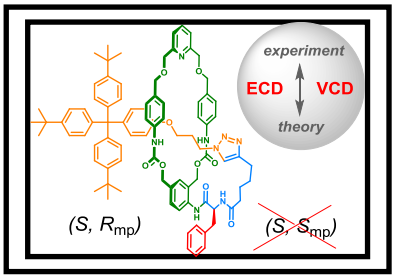

This article reports the absolute configuration of an enantiopure [1]rotaxane determination by comparing experimental *vs.* theoretical ECD and VCD spectra.